Low-Temperature Phase Transformation from Graphite to sp^{3} Orthorhombic Carbon

Jian-Tao Wang, Changfeng Chen, and Yoshiyuki Kawazoe

Phys. Rev. Lett. **106**, 075501 — Published 16 February 2011

DOI: 10.1103/PhysRevLett.106.075501

Low-Temperature Phase Transformation from Graphite to sp^3-orthorhombic Carbon

Jian-Tao Wang,[1,2,*] Changfeng Chen,[2] and Yoshiyuki Kawazoe[3]

[1]*Beijing National Laboratory for Condensed Matter Physics, Institute of Physics, Chinese Academy of Sciences, Beijing 100190, China*
[2]*Department of Physics and HiPSEC, University of Nevada, Las Vegas, Nevada 89154, USA*
[3]*Institute for Materials Research, Tohoku University, Sendai, 980-8577, Japan*

(Dated: January 11, 2011)

We identify by *ab initio* calculations an orthorhombic carbon polymorph in *Pnma* symmetry that has the lowest enthalpy among proposed cold-compressed graphite phases. This new phase contains alternating zigzag and armchair buckled carbon sheets transformed via a one-layer by three-layer slip mechanism. It has a wide indirect band gap and a large bulk modulus that are comparable to those of diamond. Its simulated x-ray diffraction pattern best matches the experimental data. Pressure plays a key role in lowering the kinetic barrier during the phase conversion process. These results provide a comprehensive understanding and an excellent account for experimental findings.

PACS numbers: 61.50.Ks, 61.66.Bi, 62.50.-p, 63.20.D-

Carbon exhibits numerous phases with distinct sp^2- and sp^3-hybridized bonds [1]. Without catalysts, graphite can be converted to hexagonal and cubic diamond at pressures above 15 GPa and temperatures above $\sim$ 1300 K [2–7]. Molecular dynamics studies [8] have shown that graphite layers first shift relative to one another under high pressure and then abruptly buckle, yielding a mixture of cubic and hexagonal diamonds. On the other hand, cold compression of graphite at room temperature produces a transparent and hard phase [9–15] distinct from hexagonal and cubic diamond. It is characterized by a marked increase in electrical resistivity from metal to insulator [9–13] above 15 GPa, an increase in optical transmittance above 18 GPa [9, 10], a broadening of the higher frequency E_{2g} Raman line [15], and changes in the x-ray diffraction (XRD) patterns above 14 GPa [11–14]. Recent theoretical studies have proposed several new structures for such cold-compressed graphite [16–18], including the monoclinic M-carbon [17] and the body-centered tetragonal bct-C_4 carbon [18]. However, despite these findings, the atomistic mechanisms for the phase transformation and the lowest-enthalpy structural conversion paths remain largely unexplored [19].

In this Letter, we present a comprehensive study of the energetics and kinetics for the phase conversion of graphite under a wide pressure range of 5 $\sim$ 25 GPa. We pay special attention to the initial reconstruction processes along various sliding and buckling pathways of the carbon sheets. We find that cold-compressed graphite tends to form an sp^3-orthorhombic *Pnma* structure (named orthorhombic W-carbon hereafter) with alternating zigzag and armchair buckled carbon sheets via a one-layer by three-layer slip mechanism. Throughout the conversion process, pressure plays a key role in lowering the kinetic barrier by establishing and maintaining energetically favorable bond reconstruction between carbon sheets. This new phase is more favorable than the previously proposed bct-C_4 and monoclinic M-carbon in terms of both energetics (enthalpy) and kinetics (enthalpy barrier), and also better matches the experimental x-ray diffraction pattern.

The calculations were carried out using the density functional theory within the local density approximation (LDA) as implemented in the Vienna *ab initio* simulation package (VASP) [20]. The all-electron projector augmented wave (PAW) method [21] was adopted with $2s^2 2p^2$ treated as valence electrons. A plane-wave basis set with an energy cutoff of 800 eV was used and gave well converged total energy of $\sim$1 meV per atom. Forces on the ions are calculated through the Hellmann-Feynman theorem allowing a full geometry optimization. The phase transitions are simulated using the climbing image nudged elastic band (CI NEB) method [22]. Phonon calculations are performed using the package MedeA [23] with the forces calculated from VASP.

We first characterize the structural, electronic and mechanical properties of the new W-carbon phase. Its crystal structure with the space group *Pnma* (D_{2h}^{16}) is shown in Fig. 1(a). At zero pressure, the equilibrium lattice parameters are a = 8.979 Å, b = 2.496 Å, and c = 4.113 Å with four inequivalent crystallographic sites, occupying the 4c (0.1952, 0.75, 0.0755), (0.1895, 0.25, 0.3010), (0.5207, 0.25, 0.0914), and (0.4633, 0.25, 0.4316) positions, respectively. By fitting the calculated total energy as a function of volume to the third-order Birch-Murnaghan equation, we obtain the bulk modulus (B_0) of W-carbon as 444.5 GPa, which is larger than that of c-BN (396 GPa) [24] and very close to the value for diamond (466 GPa). At high pressures, W-carbon becomes stable relative to graphite above 12.32 GPa [Fig. 1(b)], and is more stable (i.e., lower in enthalpy) than both bct-C_4 and M-carbon.

The electronic band structure of W-carbon at 15 GPa is shown in Fig. 1(c). The valence band top is at the Γ point and the conduction band bottom is at the T point. The LDA band gap is 4.39$\sim$4.52 eV over a wide

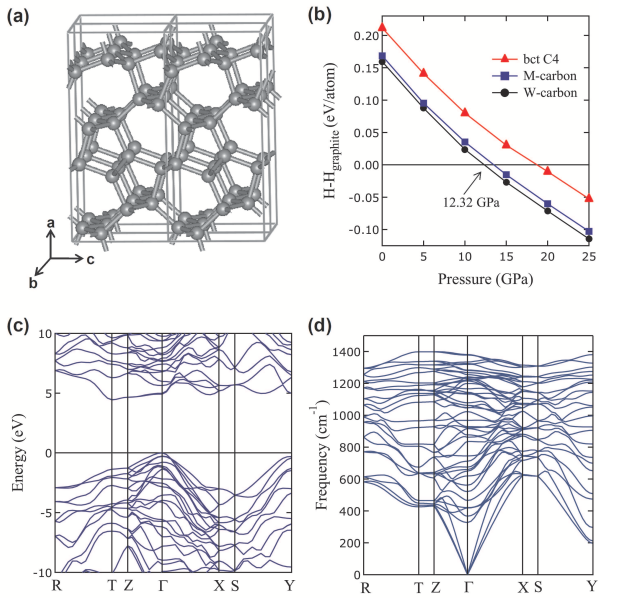

FIG. 1: (color online). Properties of the orthorhombic W-carbon in $Pnma$ symmetry. (a) Polyhedral views of the crystal structure; (b) The enthalpy per atom for bct-C_4 [18], M-carbon [17], and W-carbon as a function of pressure relative to graphite. (c) Calculated electronic band structure of W-carbon at 15 GPa. (d) Calculated phonon dispersion curves of W-carbon at 15 GPa.

pressure range of 0∼25 GPa, which is remarkably larger than the value of 2.56 eV for bct C_4 [18] and 3.60 eV for M-carbon [17]; it is even appreciably larger than the LDA gap (4.17 eV) [25] for diamond. Therefore, W-carbon is expected to be optically transparent in agreement with experiments [1].

We have calculated its phonon dispersion curves within a wide pressure range up to 40 GPa. No imaginary frequencies were observed throughout the whole Brillioun zone [results at 15 GPa are shown in Fig. 1(d)], confirming dynamical stability of the sp^3-orthorhombic W-carbon. The calculated volume, bulk modulus and band gaps at zero pressure are listed in Table I and compared to available experimental data [26] for diamond and calculated data for bct-C_4 [18] and M-carbon [17]. These results provide an excellent account for the *transparent and superhard* cold-compressed graphite phase [1, 14].

We now study the atomistic processes underlying the transformation from graphite toward the W-carbon and other compressed phases. We have examined various sliding-buckling processes along the low-index orientations [100] and [210] of graphite. The orthorhombic W-carbon is formed by alternating zigzag and armchair buckling via a one-layer (A1) by three-layer (B1,A2,B2) slip model along the [100] orientation (Fig. 2a); M-carbon is formed by alternating zigzag and armchair buckling via a two-layer (A1,B1) by two-layer (A2,B2) slip model along the [100] orientation (Fig. 2b); the bct-C_4 phase is obtained by a one-layer (A1) by one-layer (B1) slip model along the [210] orientation with armchair buckling (Fig. 2c). For comparison, we also considered the pathways to form hexagonal diamond (hex-d) and cubic diamond (cub-d). Hex-d is obtained by a one-layer (A1) by one-layer (B1) slip model along the [210] orientation via an orthorhombic configuration (Fig. 2d) with a stacking different from that for bct-C_4; cub-d is obtained by a two-layer (A1,B2) by two-layer (B1,A2) slip model along the [100] orientation with zigzag buckling (Fig. 2e) that is different than M or W-carbon. Here the pathway to form hex-d with armchair buckling [8] is consistent with the experimental findings that the c-axis of hex-d is perpendicular to the original c-axis of hex-g [11], and the pathway to form cub-d with zigzag buckling [8] leads to the final [112] diamond orientation parallel to the c axis of the hex-g, which is consistent with the results of shock-wave experiments [27]. These pathways are simulated using the CI NEB method [22] with an 8-atom, or 16-atom supercell containing two carbon sheets for bct-C_4, hex-d, or four carbon sheets for cub-d, M-carbon and W-carbon. No symmetry constraint was imposed in the structural optimization procedure.

TABLE I: Calculated equilibrium volume (V_0 in Å^3/atom), bulk modulus (B_0 in GPa) and band gaps (E_g in eV) for diamond, bct-C_4, M, and W-carbon at zero pressure, compared to available experimental data [26] for diamond and calculated data for bct C_4[18] and M-carbon [17].

Structure	Method	V_0 (Å^3)	B_0 (GPa)	E_g (eV)
Diamond	this work	5.52	466.3	4.20
	LDA[17]	5.52	468.5	
	LDA[25]			4.17
	Exp[26]	5.67	446	5.47
M-carbon	this work	5.79	438.7	3.56
	LDA[17]	5.78	431.2	3.60
bct C_4	this work	5.83	433.7	2.58
	LDA[18]	5.82	428.7	2.56
W-carbon	this work	5.76	444.5	4.39

Figure 3(a) shows the enthalpy along the pathways toward the formation of W-carbon, M-carbon, bct-C_4, hex-d and cub-d at 15 GPa. We note that graphite's layered structure makes the sliding and buckling of the carbon layers relatively easy to occur at the early stages of structural transformation under compression. Among various sliding and buckling modes, the pathway toward the W-carbon phase has the lowest enthalpy up to step 20 as shown in Fig. 3(a) at 15 GPa. In fact, the initial sliding and buckling along the W-carbon pathway is expected to be favored to happen at relatively low pressure below 15 GPa. Consequently, the original starting graphite structure would be turned into a new layered carbon structure with sliding and buckling patterns sim-

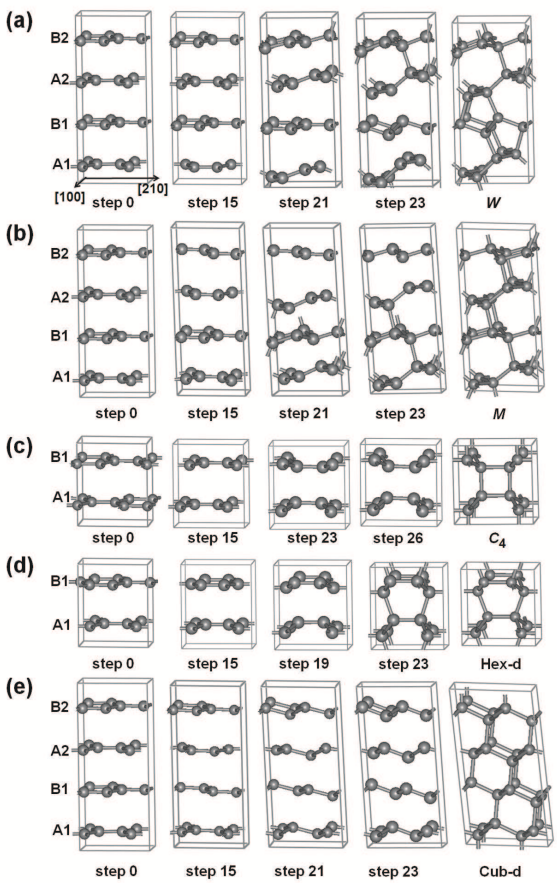

FIG. 2: (color online). Pathways to form W-carbon (a), M-carbon (b), bct-C_4 (c), hex-d (d) and cub-d (e) starting from graphite with distinct sliding-buckling processes of carbon sheets along the [100] or [210] orientations of graphite.

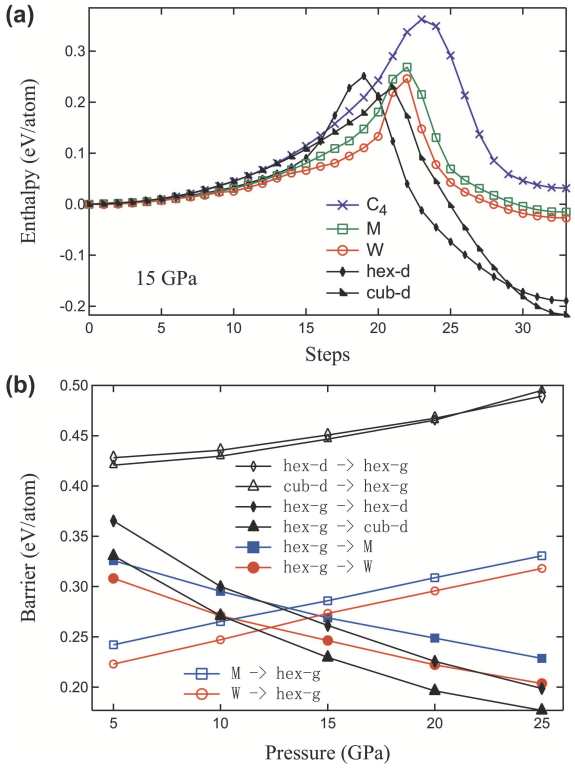

FIG. 3: (color online). (a) Enthalpy versus pathway at 15 GPa for the transformations shown in Fig. 2. (b) Enthalpy barriers versus pressure. The solid and open symbols represent the reaction and counter-reaction barriers, respectively.

ilar to those shown in Fig. 2(a) early on under cold compression. This new layered carbon structure along the W-carbon pathway (a "pre-W-carbon" layered structure) can be regarded as the new "starting phase" for further phase transformation under higher pressure. From this pre-W-carbon structure, further phase transformation can either proceed directly toward the W-carbon phase with a relatively low total barrier of 0.246 eV (at 15 GPa, same below) or cross over to a different pathway with a higher cross-path barrier. For example, crossing over to the pathway toward the hex-d structure from the pre-W-carbon at the point where the two paths intersect [around step 21 in Fig. 3(a)] would encounter an additional cross-path barrier of 0.128 eV, resulting in a much higher total barrier of about 0.336 eV for the cross-path transition to hex-d structure. The situation is similar for cross-path transitions to other structures. Therefore, the transformation toward W-carbon is favored under cold compression, which is in agreement with the experimental observation (see below). Meanwhile, at high temperatures, thermal energy should overcome the additional cross-path barrier or the initial higher-enthalpy cost of the pathways toward diamond phases, which is consistent with the experimental observation that graphite is converted to hex-d only at high pressures and high temperatures above 15 GPa and 1300 K [2–7].

We plot in Fig. 3(b) the enthalpy barriers versus pressure. With increasing pressure from 5 to 25 GPa, the barriers decrease from 0.365 to 0.199 eV for hex-g → hex-d, 0.331 to 0.177 eV for hex-g → cub-d, 0.326 to 0.229 eV for hex-g → M-carbon, and 0.308 to 0.203 eV for hex-g → W-carbon. These results demonstrate that pressure plays a key role in lowering the kinetic barrier and facilitates the phase transformation. In particular, the barrier toward the W-carbon is the lowest up to about 10 GPa and remains competitive at higher pressures.

Experimentally, the sp^3-bonded *transparent phase* of carbon has been found to be reversible with release of pressure at room temperature [1, 7, 11, 14]. To clarify this point, we have examined the counter-reaction barrier from M- and W-carbon to revert to graphite [see Fig. 3(b)]. With release of pressure from 25 to 5 GPa, the counter-reaction barriers are reduced from 0.331 to 0.242 eV for M-carbon → hex-g, and 0.318 to 0.223 eV for W-carbon → hex-g. These results underscore the key role of pressure in stabilizing the W- or M-carbon under compression and making them easily revert back to

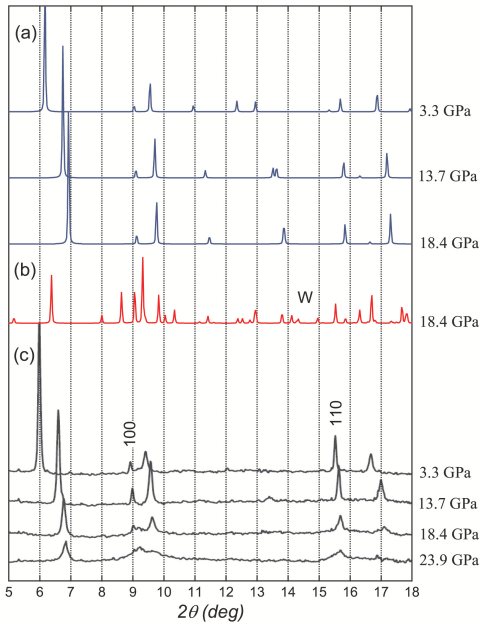

FIG. 4: (color online). (a) Simulated XRD patterns of graphite at 3.3, 13.7 and 18.4 GPa. (b) Simulated XRD patterns of W-carbon at 18.4 GPa. (c) Experimental XRD patterns [14]. X-ray wavelength is 0.3329 Å.

graphite upon the release of pressure.

Figure 4 shows the simulated XRD patterns of graphite and W-carbon, compared to the experimental ones at various pressures [14]. The strongest peaks for W-carbon are located in the region between 8.5−10.5 deg and 15−17 deg, which correspond almost exactly to where pressure-induced broad peaks appear in the experimental results. The relatively weaker peaks of W-carbon and graphite in the range of 11−14 deg have merged into the background, and the peaks of W-carbon in the range of 6−7 deg have combined with those from graphite into a broadened peak. The experimental high pressure phase [1, 14] was argued to have both σ- and π-bonding, which can be attributed to the coexistence of a mixture of graphite and W-carbon. We note that a possible (3,0)/(4,0)ab phase with π-bonding [16] has been proposed; however, it is unstable and likely to form a more stable sp^3-(4+6+8) ring structure with an energy gain of 0.05 eV per atom. Considering the very low compressibility of W-carbon, the marked change of the experimental XRD patterns from 13.7 to 23.9 GPa are attributed to the increase of ratio of W-carbon in the graphite phase. This highlights the dual role of pressure in lowering the conversion barrier and enhancing the production of the compressed phase [14].

In summary, we have performed a comprehensive study of the lowest-enthalpy structures and the phase transformation mechanisms for cold-compressed graphite using *ab initio* calculations. Our results reveal that at low temperatures the phase transformation initiates and proceeds along the pathways with lowest enthalpy toward a newly identified sp^3-orthorhombic W- or previously proposed monoclinic M-carbon phases with distinct alternating zigzag and armchair buckling of carbon sheets. The present results provide an excellent account for the experiment on the cold-compressed graphite; they also provide insights for understanding high-temperature phase transformation pathways for carbon structures.

This study was supported by the NSFC of China (Grant No. 10974230) and CAS (Grant No. KJCX2-YW-W22). C.F.C acknowledges support by DOE under Cooperative Agreement DE-FC52-06NA27684. Acknowledgment goes to Prof. Motoko Kotani. We are thankful to the crew of the Center for Computational Materials Science at IMR, Tohoku University for their support at the SR11000 supercomputing facilities.

* e-mail address:wjt@aphy.iphy.ac.cn

[1] E. D. Miller, D. C. Nesting, and J. V. Badding, Chem. Mater. **9,** 18 (1997).
[2] R. B. Aust and H. G. Drickamer, Science **140,** 817 (1963).
[3] R. Clarke and C. Uher, Adv. Phys. **33,** 469 (1984).
[4] H. Sumiya and T. Irifune, J. Mater. Res. **22,** 2345 (2007).
[5] T. Irifune, *et al.*, Nature (London) **421,** 599 (2003).
[6] F. P. Bundy, *et al.*, Carbon **34,** 141 (1996).
[7] F. P. Bundy and J. S. Kasper, J. Chem. Phys. **46,** 3437 (1967).
[8] S. Scandolo, M. Bernasconi, G. L. Chiarotti, P. Focher, and E. Tosatti, Phys. Rev. Lett. **74,** 4015 (1995).
[9] W. Utsumi and T. Yagi, Science **252,** 1542 (1991).
[10] M. Hanfland, K. Syassen, and R. Sonnenschein, Phys. Rev. B **40,** 1951 (1989).
[11] T. Yagi, W. Utsumi, M. A. Yamakata, T. Kikegawa, and O. Shimomura, Phys. Rev. B **46,** 6031 (1992).
[12] K. J. Takano, H. Harashima, and M. Wakatsuki, Jpn. J. Appl. Phys. **30,** L860 (1991).
[13] Y. X. Zhao and I. L. Spain, Phys. Rev. B **40,** 993 (1989).
[14] W. L. Mao, *et al.*, Science **302,** 425 (2003).
[15] M. Hanfland, H. Beister, and K. Syassen, Phys. Rev. B **39,** 12598 (1989).
[16] F. J. Ribeiro, S. G. Louie, M. L. Cohen, and P. Tangney, Phys. Rev. B **72,** 214109 (2005).
[17] Q. Li, *et al.*, Phys. Rev. Lett. **102,** 175506 (2009).
[18] K. Umemoto, R. M. Wentzcovitch, S. Saito, and T. Miyake, Phys. Rev. Lett. **104,** 125504 (2010).
[19] X. F. Zhou, *et al.*, Phys. Rev. B **82,** 134126 (2010).
[20] G. Kresse and J. Furthmüller, Phys. Rev. B **54**, 11169 (1996); G. Kresse and J. Hafner, *ibid.* **47**, 558 (1993).
[21] P. E. Blöchl, Phys. Rev. B **50**, 17953 (1994); G. Kresse and D. Joubert, Phys. Rev. B **59**, 1758 (1999).
[22] http://theory.cm.utexas.edu/henkelman.
[23] K. Parlinski, Z-. Q. Li, and Y. Kawazoe, Phys. Rev. Lett. **78,** 4063 (1997).
[24] A. F. Goncharov, *et al.*, Phys. Rev. B **75,** 224114 (2007).
[25] W. G. Aulbur, M. Stadele, and A. Gorling, Phys. Rev. B **62,** 7121 (2000).
[26] F. Occelli, P. Loubeyre, and R. Letoullec, Nature Mater. **2,** 151 (2003).

[27] E. J. Wheeler and D. Lewis, Mat. Res. Bull. **10,** 687 (1975).